Spin-Mass Interaction Low-Temperature Experiment on ISS

Ho Jung Paik and M. Vol Moody
Department of Physics, University of Maryland, College Park, MD 20742

Donald M. Strayer
Jet Propulsion Laboratory, 4800 Oak Grove Drive, Pasadena, CA 91109

The objective of SMILE (Spin-Mass Interaction Low-temperature Experiment) is to search for interaction between intrinsic spin of particles and mass. SMILE is an ISS experiment capable of approaching, to within a factor of 100, the spin-mass interaction allowed for the axion. The Brownian motion provides the ultimate limit of sensitivity for a gravity experiment. The low-g environment of space permits nearly free suspension of the test mass, under which the highest resonance quality factor can be attained, limited only by interaction with residual gas molecules. SMILE employs a superconducting differential angular accelerator, a very sensitive force sensor. The differential accelerometer is capable of rejecting the accelerations of the platform to extremely high precision. The spin source is an elongated toroid with alternating sections formed from two high-permeability materials with different saturation spin densities.

1. Objectives of SMILE

Several modern theories predict the existence of light-mass pseudoscalar bosons, which should give rise to a force between intrinsic spin and mass. The best motivated of such bosons, the *axion*, appears in the well-known Peccei-Quinn (1977) solution to the "strong CP problem" of particle physics. For an electron with spin polarized in the direction $\hat{\sigma}$ and an unpolarized nucleon, the interaction potential is given (Moody and Wilczek, 1984) by

$$V_a = g_s g_p \frac{\hbar^2}{8\pi m_e}(\hat{\sigma}\cdot\hat{r})\left(\frac{1}{\lambda r}+\frac{1}{r^2}\right)e^{-r/\lambda}, \tag{1}$$

where m_e is the mass of the electron, $\hat{r}$ is the unit position vector of the nucleon relative to the electron, and λ is the range of the force, which is inversely proportional to the axion mass. The dimensionless coupling constants g_s and g_p are related to θ and λ (Blaser *et al.*, 1996) by

$$g_s g_p \cong \frac{\theta}{\lambda^2}\times 6\times 10^{-33}, \tag{2}$$

where θ is a dimensionless angle $\leq 3 \times 10^{-10}$ and λ is in meters.

The best direct limit on $g_s g_p$ at short range comes from the experiment of Ni *et al.* (1999): $g_s g_p < 1 \times 10^{-28}$ for $\lambda \geq 3$ cm. SMILE (Spin-Mass Interaction Low-temperature Experiment) aims at approaching the axion limit to within two orders of magnitude at $\lambda = 1$ mm. Although the experiment may fall short of actually detecting the axion, it will search for generic spin-mass coupling mechanisms 10^8 times weaker than currently observable. A positive result would constitute the discovery of a new interaction in nature, and would have a major impact in particle physics and astrophysics.

Figure 1 shows the expected resolution of SMILE versus λ. Also shown are the best existing limit by , the theoretical upper limit for the axion, and the expected resolution of our ground experiment, and the potential sensitivity of a free-flyer experiment. SMILE will demonstrate many crucial components of the ultimate free-flyer experiment, including the high Q of the test masses in micro-g and the acceleration rejection capability of the detector.

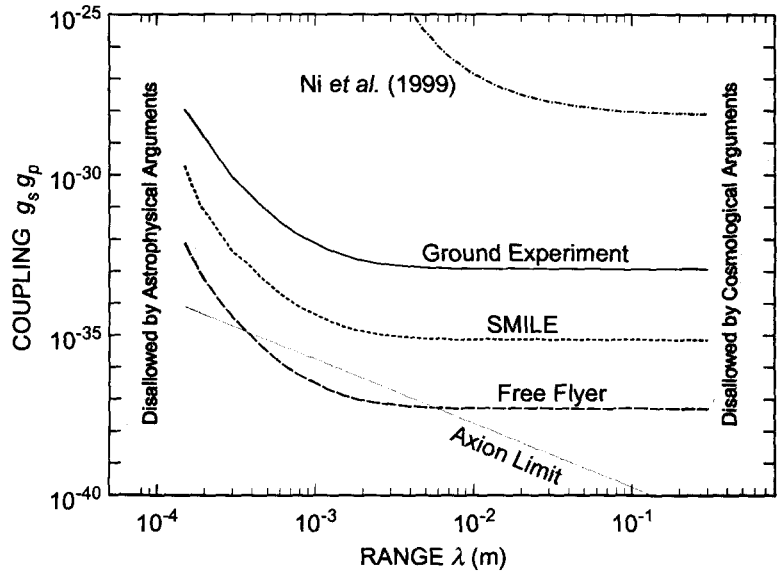

Figure 1. Sensitivity of SMILE versus the existing limit.

2. Scientific Value of Spin-Mass Coupling Experiment

Test of General Relativity. The existence of a spin-mass coupling implies a violation of the Equivalence Principle, a cornerstone of General Relativity. Although STEP (Satellite Test of the Equivalence Principle) aims at extending the limits of the Equivalence Principle to one part in 10^{18}, the spin-coupling violation cannot be detected by STEP, since it uses unpolarized test masses. Thus SMILE complements STEP in testing General Relativity.

Strong CP problem. The Standard Model of particle physics successfully accounts for all existing particle data; however, it has one serious blemish: the strong *CP* problem. Strong interactions are such that parity (*P*), time reversal (*T*), and charge conjugation (*C*) symmetries are automatically conserved in perturbation theory. However, non-perturbative effects induce violations of *P* and *CP*, parameterized by θ. The *a priori* expectation of θ is of the order of unity, but no violations of *P* or *CP* have been observed in strong interactions. In particular, present upper bounds on the neutron electric dipole moment (Altarev *et al.*, 1992) require $\theta \leq 3 \times 10^{-10}$. Peccei and Quinn (1977) developed an attractive resolution of this problem. One ramification of their theory is the existence of a new light-mass boson, the *axion* (Weinberg, 1978; Wilczek, 1978).

Thus, the detection of spin-mass coupling at the level predicted by axion models would provide the first direct experimental confirmation of a solution to the serious deficiency in the Standard Model. In a more general sense, the detection of spin-mass coupling would be the first observation of macroscopic parity (*P*) and time reversal (*T*) symmetry violation.

Cold dark matter. The axion could also solve the major open question in astrophysics: the composition of dark matter. Galactic rotation curves and inflation theory require that there should be more mass in the universe than has been observed. Although neutrino mass, MACHOs (MAssive Compact Halo Objects), and many hypothetical particles have been offered as explanations, the solution remains elusive. The axion is one of the strongest candidates for the cold dark matter (Turner, 1990).

3. Principle of Experiment

Required sensitivity. The torque between a polarized source with an electron spin density ρ_s and a test mass of nucleon density ρ_N is given (Blaser *et al.*, 1996) by

$$N_a = \frac{\theta}{\lambda^2} \times 7 \times 10^{-71} \rho_s \rho_N \frac{dI}{d\theta} (\text{mks}), \qquad (3)$$

where I is the integral of the potential:

$$I = \frac{1}{8\pi} \iint (\hat{\sigma} \cdot \hat{r}) \left(\frac{1}{\lambda r} + \frac{1}{r^2} \right) e^{-r/\lambda} dV_s dV_N. \qquad (4)$$

Here the integration is performed over the volumes of the spin source and the test mass. There is some subtlety involved in the design of a spin source. The integral I vanishes identically for any closed loop of spin (Shaul *et al.*, 1996). Thus, a source with alternating materials is needed, with the greatest possible contrast in spin density.

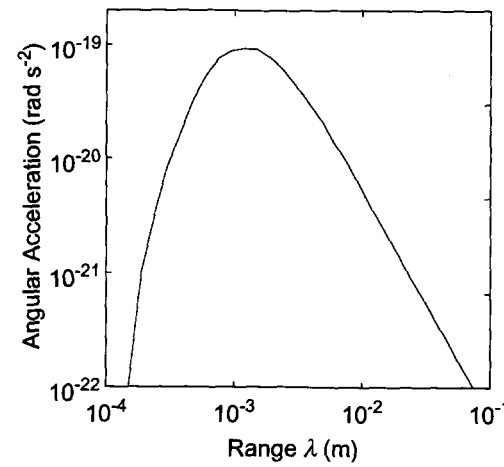

Figure 2. Angular acceleration corresponding to $\theta = 3 \times 10^{-10}$ as a function of λ.

Figure 2 shows the angular acceleration signal computed for our source and detector design as a function of λ for $\theta = 3 \times 10^{-10}$. A maximum differential angular acceleration signal of 1.0×10^{-19} rad s^{-2} occurs at $\lambda \sim 1$ mm. To achieve the required sensitivity, the intrinsic noise of the instrument as well as its isolation from seismic, gravitational, and electromagnetic disturbances must be improved by several orders of magnitude over existing devices.

Spin source. Figure 3 shows the cross section of the spin source and a test mass perpendicular to the rotation axis, along with associated coils. The source is an elongated toroid with 32 alternating sections formed from two high-permeability materials with different saturation spin densities. Sixteen ridges on the inner surface of the test mass shell allow coupling to the spin source. To generate a differential torque, the ridges of test mass 1 are aligned with material A while those of test mass 2 are aligned with material B. A low-frequency current through toroidal windings modulates the spins in the source materials. A superconducting shield (not shown) isolates the test masses from the magnetic field of the source.

Detector. The detector consists of two identical angular accelerometers. The test masses are magnetically levitated and have cylindrical symmetry to high order. Due to its quantum nature, superconducting magnetic levitation is *extremely stable*, permitting a very high passive common-mode rejection ratio (CMRR) to be maintained.

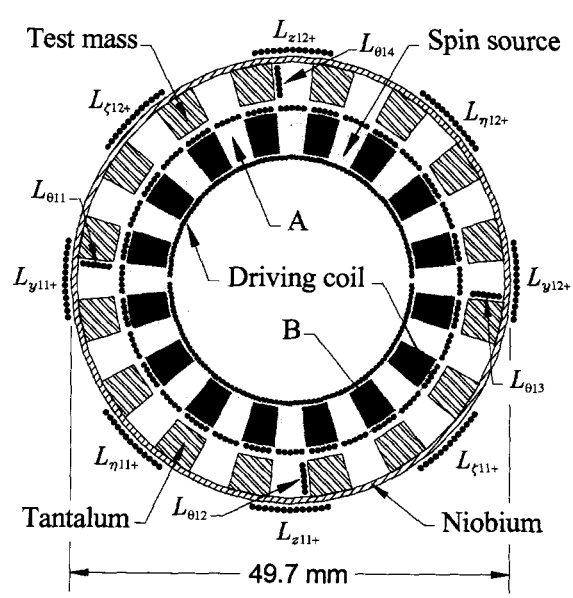

Figure 3. Cross section of the spin source and one test mass with alignment and sensing coils.

Figure 4 shows a cross section of the spin source and test masses parallel to the rotation axis. Coils coupled to the outer surfaces of the test masses permit alignment of the accelerometer sensitive axes as well as detection of the linear and angular acceleration of the platform. The two test masses are coupled together through the rotation sensing coils, facing their ridges (see Figure 3), to form a differential angular accelerometer.

Due to the *cylindrical symmetry*, the forces applied by the external coils do *not* couple to the test mass angular degree of freedom about the sensitive axis. Further, an angular accelerometer is intrinsically insensitive to forces arising from the charge on the test mass and temperature gradient across the instrument.

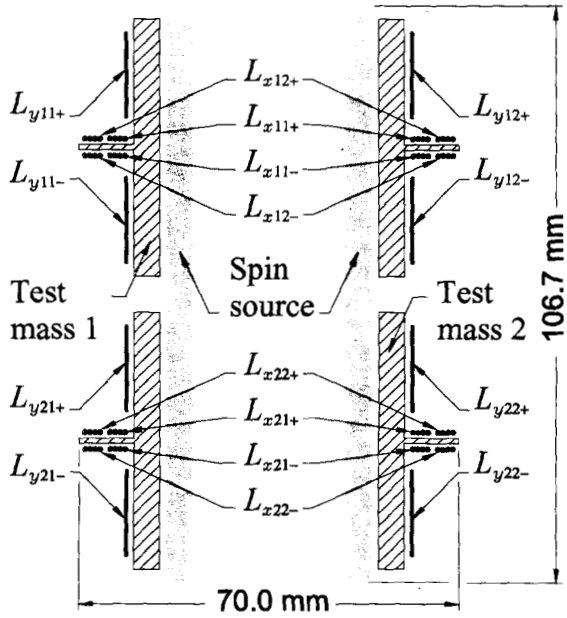

Figure 4. Cross sectional view of the apparatus along with suspension and alignment coils.

4. Experimental Hardware

Overview of the apparatus. The spin source is completely wrapped with a niobium (Nb) shield. Two sensing coil forms are mounted on the middle flange outside the shield, and the two test masses ride on these coil forms. Outside the test masses, four alignment coil forms are assembled and mounted on the middle flange. The entire apparatus is fastened to the second-stage thermal platform of the Cryo Insert, with its long axis pointing along-track (x-axis) (Figure 5). The temperature of the platform is stabilized to 5 μK. The basic cryogenic requirements of

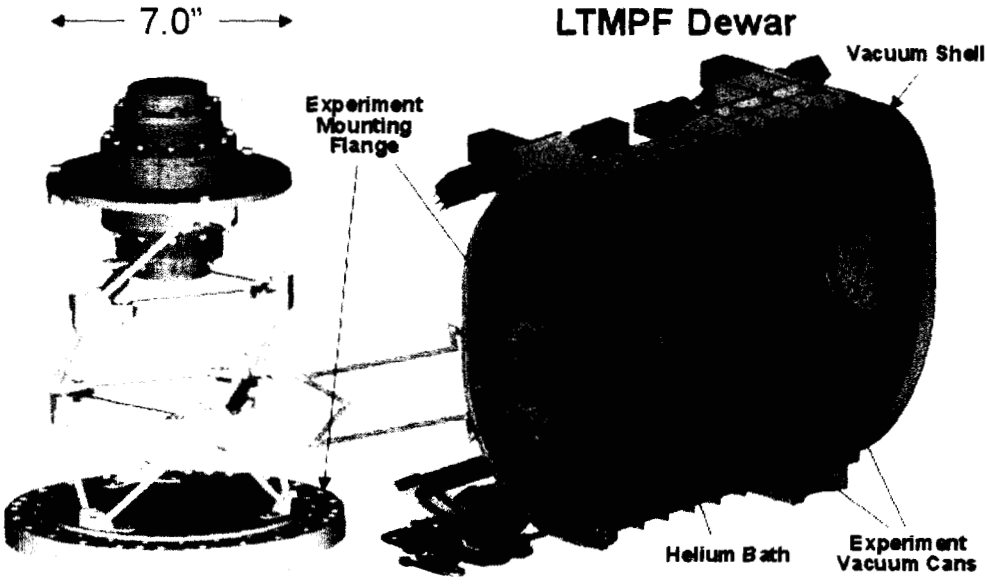

Figure 5. The ISP mounted on the Cryo Insert and the LTMPF dewar.

SMILE are met by the standard provision of LTMPF. The main upgrade required is adding a cryopump to reduce the pressure to 10^{-10} torr. Due to the excellent CMRR of the superconducting differential accelerometer, SMILE does not require vibration isolation.

Spin source. For transition metals, crystal field quenching of orbital angular momentum, L, implies that total atomic angular momentum, J, approximately equals the intrinsic spin, S. Below the Curie temperature, ρ_S is given by $2M/g\mu_B$, where M is the magnetization, g is the spectroscopic splitting factor (≈ 2), and μ_B is the Bohr magneton. Hence, materials with similar magnetizations will have similar spin densities. The solution lies in the use of materials containing rare-earth elements. The rare-earth elements below gadolinium (Gd) are particularly interesting, because for these, $J = L - S$, so the intrinsic spins are anti-parallel to the magnetization.

Newman (1983) used this concept in a toroidal spin source consisting of NdNi and $GdNi_5$. For SMILE, we propose to combine NdNi with Magnifer 7904 (80% Ni, 14% Fe, 5% Mo), a soft high-μ transition metal. The source is designed such that Magnifer completely shields NdNi, intercepting any magnetic field from it. The saturation magnetic field of Magnifer is ~ 0.75 T. When driven to an amplitude of 0.35 T, ρ_s will be modulated to 2.9×10^{28} m^{-3} for NdNi (Graham, 1987) and 3.0×10^{28} m^{-3} for Magnifer, with opposite spin directions. This results in the angular acceleration signal plotted in Figure 2.

The main structure pf the source is machined out of Magnifer. Along the length of the toroid, 16 identical, evenly distributed, pockets are machined using wire EDM (electric discharge machine). NdNi is melted and poured into the pockets in the Magnifer form. A Nb coil is wound toroidally about the source to provide the charging field. A 0.38-mm thick Nb tube shields test masses from the magnetic field in the spin sources. To reduce the crosstalk between the leads, the source will be driven with a small external current through a superconducting transformer located inside the toroid.

Test masses. The test mass will have 16 ridges which interact with the source. To obtain a large nucleon density ($\rho_N = 1.00 \times 10^{31}$ m^{-3}), the ridges will be fabricated out of tantalum (Ta), a type-I superconductor of high density (16.6 g cm^{-3}), with a relatively high transition temperature and critical field. However, to minimize the stray mass, the rest of the test mass will be made out of Nb, a lighter material (8.57 g cm^{-3}) with excellent superconducting properties. This design gives a mass of 0.28 kg and a moment of inertia of $I = 1.5 \times 10^{-4}$ kg m^2.

Two prototype test masses have been machined out of a single block of Nb, by turning the outer surfaces on a lathe and then cutting the ridges with a wire EDM (see Figure 6). To fabricate a SMILE test mass, a Ta cylinder will first be tightly fitted inside a Nb shell and diffusion-bonded. The rest of the machining will follow the procedure established for the prototype.

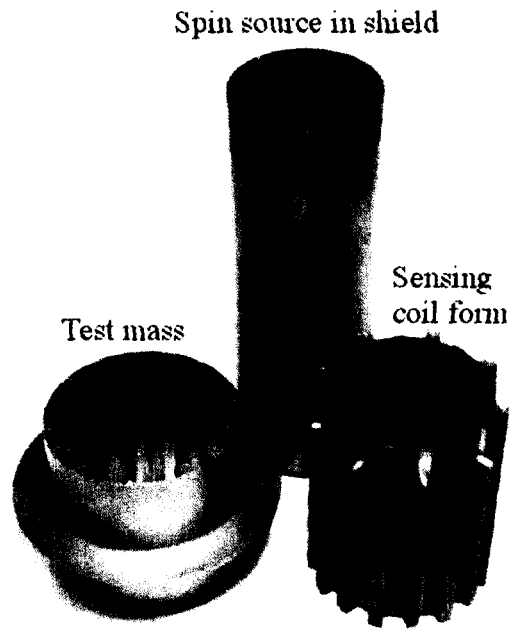

Figure 6. Photograph of the prototype spin source, test mass, and sensing coil form.

General requirements for the circuits. The superconducting circuits used in SMILE are of the type fully analyzed and tested in our superconducting gravity gradiometer (SGG) project (Chan and Paik, 1987; Chan *et al.*, 1987). A new feature is the feedback circuits provided for the auxiliary accelerometers, which are required to actively stiffen and damp resonant modes of the test masses. The linearity requirement of the differential accelerometer is met without feedback.

In general, higher sensitivity can be achieved by reducing the resonance frequency of an accelerometer. On the other hand, the nonlinearity of scale factors, which couples in the platform noise, favors stiffer suspension. We choose a compromise solution: the differential-mode (DM) and common-mode (CM) frequencies of f_D = 0.01 Hz and f_C = 0.04 Hz, respectively. This choice is also partially to take advantage of the quietest noise spectrum of the ISS at ~ 0.01 Hz.

The translational modes can be tuned to higher frequencies to reduce the displacements of the test masses. However, the test masses must be left as free as possible to obtain the highest Q for the accelerometer. We choose ~ 0.2 Hz, the minimum frequency required to keep the random excursion of the test masses to ≤ 10 μm, 10% of the coil gaps. The modes are then stiffened *actively* to ~100 Hz to suppress the nonlinearity noise.

Suspension and alignment circuits. Two concentric pancake coils ($L_{xj1\pm}$'s in Figure 4) face either side of each test mass flange. Two inner coils are coupled in the circuit shown in Figure 7(a) to provide axial suspension. The two SQUIDs detect linear acceleration a_x and gravity gradient Γ_{xx} along the x-axis. Two outer coils ($L_{xj2\pm}$'s in Figure 4) are coupled in an identical circuit (not shown), except that the SQUIDs are replaced by the leads for feedback currents. This circuit will stiffen and damp the CM and DM along the x-axis.

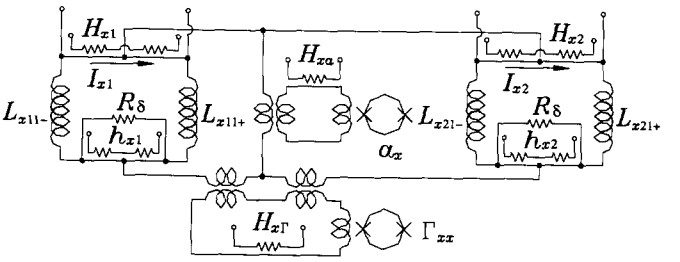

(a) Axial suspension circuit

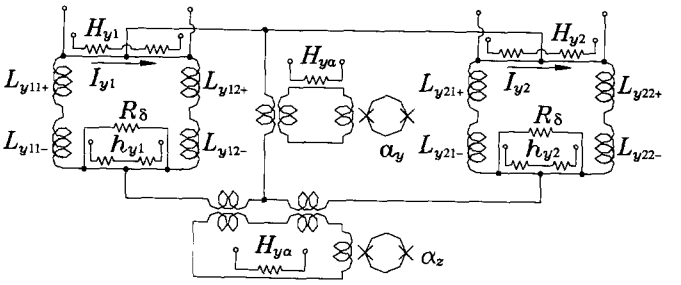

(b) Radial suspension circuit

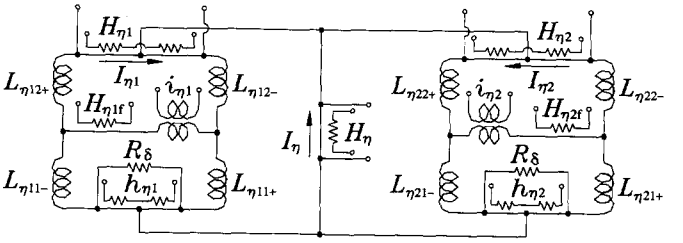

(c) Angular alignment circuit

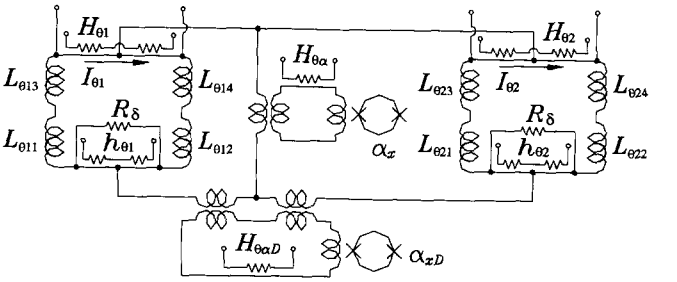

(d) Signal sensing circuit

Figure 7. Superconducting circuits for SMILE.

Eight curved pancake coils are symmetrically located about the outer surface of the cylinder on either side of the flange. The coils at 0° and 90° angles ($L_{yij\pm}$'s and $L_{zij\pm}$'s in Figure 3) are connected to suspend the radial degrees of freedom. Figure 7(b) is a schematic of the suspension circuit for the y-axis. The SQUIDs detect linear acceleration a_y and angular acceleration α_z.

To remove coupling to cross-component angular accelerations, the accelerometer axes must be aligned precisely. The coils located at 45° angles ($L_{\eta ij\pm}$'s and $L_{\zeta ij\pm}$'s in Figure 3) are used to provide this alignment. Figure 7(c) is the alignment circuit for the $y = z$ plane. This circuit is also used to control the angular motion about the $y = -z$ axis and the linear motion along the $y = z$ axis. The signals from the radial suspension circuits are mixed with proper scale factors and fed back to the feedback transformers to stiffen and damp both the linear and angular modes.

Angular acceleration sensing circuit. Four elongated pancake coils ($L_{\theta ij}$'s in Figure 3) are provided for each test mass to sense the angular motion about the symmetry axis. These coils are connected in a circuit shown in Figure 7(d) to form a differential angular accelerometer. The two SQUIDs sense the common (α_x) and differential (α_{xD}) angular acceleration about the x-axis. The current ratio, $I_{\theta 2}/I_{\theta 1}$, is adjusted to balance out the CM from the DM output. With the angular modes not actively controlled, the DM of $Q_D = 10^{10}$ implies a decay time of 10 years! The SQUID protection heat-switches, $H_{x\alpha}$ and $H_{x\alpha D}$, are turned on when the modes get excited.

To wind the elongated pancake coils, the coil form holder is cut from Nb by wire EDM. In four orthogonal ridges, pockets are removed and filled with Stycast epoxy (see Figure 6) such that, when a coil is wound, it is partially on the Nb and partially on the epoxy. The part on the epoxy is the active component of the coil, which senses the angular displacement of the test mass. The coils have been successfully fabricated using this procedure for the ground apparatus.

Coarse and fine heat-switches. Due to the high vibration levels of ISS, a special provision must be made to be able to fine control the magnetic fluxes trapped in various superconducting loops. While a current is sent from a current source to a circuit, a test mass undergoes a random excursion of 10 μm, which is about 10% of the nominal spacing of the coils. This means that at the moment the heat-switch is turned off, the coil inductance, hence the trapped flux, is uncertain to 10%, regardless of the resolution of the external current supply. To overcome this problem, two sets of heat-switches are provided.

Coarse heat-switches (H_{ij}'s in Figure 7) warm up a short length of the Nb wire to a resistance $R \approx 1$ mΩ, resulting in an L/R time of about 10 ms. These switches are used to store the currents initially. Fine heat-switches (h_{ij}'s) couple a low resistance path with $R_\delta \approx 0.1$ μΩ to the circuit, resulting in a time constant of about 100 s. With 1-ms time resolution of the heat-switch, fluxes can then be adjusted to 10^{-5}. This gives the ability to match the scale factors to 10^{-5} and align the sensitive axes to 10^{-5} rad, resulting in a passive CMRR of 10^5 in all three degrees of freedom.

Dynamic error compensation. The vibration rejection capability of a superconducting differential accelerometer can be improved by compensating for the residual errors (Moody *et al.*, 1986). With linear and angular accelerations measured simultaneously, the error coefficients can be determined by shaking the platform along or about an axis and dividing the differential acceleration output by the particular acceleration component. In our laboratory SGG, the component accelerometers were balanced and aligned to 10^{-4}, which gave an initial CMRR of 10^4. Using this error compensation technique, we were able to improve both the linear and angular acceleration rejection by a factor of 10^3 to a CMRR of 10^7 (Moody *et al.*, 2002).

Applying the same gain to the SMILE detector, we should be able to achieve a CMRR of 10^8 for angular acceleration. Due to the cylindrical symmetry, the outer coils cannot convert the linear acceleration of the platform into a torque on the test masses. The linear acceleration does couple, however, to the angular sensing circuit through mismatches in the inner sensing coils, in particular, through mismatch in the coil areas. With the expected mismatch of $\Delta A/A = 10^{-2}$ and a stiffness ratio of $(f_D/f_R)^2 = 10^{-8}$ (with feedback) between the differential angular and linear modes, the linear error coefficient for a_y and a_z becomes

$$\varepsilon_L = \left(\frac{\Delta A}{A}\right)\left(\frac{f_D}{f_R}\right)^2 \frac{1}{r_S} = 5\times10^{-8} m^{-1}, \tag{5}$$

where r_S is the radial position of the sensing coils. The error compensation reduces ε_L to 5×10^{-11} m^{-1}. The detector is insensitive to a_x.

We will use the ISS vibration noise itself to shake the detector. The accelerations will be random and cross-correlated between various degrees of freedom. However, we can apply a well-established procedure in electrical engineering for determining the transfer functions for a multiple-input system using noise alone (Bendat and Piersol, 1971).

5. Error Budget

Intrinsic instrument noise. The intrinsic noise of an accelerometer is given by the Brownian motion noise of the test masses and the noise in the readout circuit. A dc SQUID is employed as a very quiet amplifier. The effect of the amplifier noise is reduced further by conducting a *resonance* experiment. When the spin source is driven at the resonance frequency f_0 for integration time τ, the response of the test masses to both the spin-mass coupling and the Nyquist torque, as well as the back-action noise of the amplifier, increases as Q_{eff}, where Q_{eff} represents the smaller of the Q and the product $\omega_0\tau$. Since the wideband noise of the amplifier is not affected, the total amplifier contribution to the noise power is reduced by Q_{eff}.

The intrinsic power spectral density of a differential angular accelerometer, operating as a resonant detector, can be shown (Paik, 1982) to be

$$S_\alpha(f) = \frac{8\omega_0}{I}\left[\frac{k_B T}{Q} + \frac{k_B T_N}{Q_{eff}}\right], \tag{6}$$

where I is the moment of inertia and T_N is the noise temperature of the amplifier. The SQUID spec for LTMPF, 30 $\mu\Phi_0$ Hz$^{-1/2}$ with 1/f noise corner < 0.5 Hz, corresponds to $T_N \cong 1.7 \times 10^{-6}$ K at $f_0 = 10^{-2}$ Hz. With $\tau \cong 7.8 \times 10^6$ s (3 months), Q_{eff} becomes 4.9×10^4. The amplifier noise is then negligible for cases where $Q < 10^{11}$.

A crucial question is how high a Q one can achieve for weakly suspended superconducting test masses at 10^{-2} Hz. The residual gas pressure can be improved to $\leq 10^{-10}$ torr by cryopumping with activated charcoal. The limit by residual gas damping at 10^{-10} torr is $Q \approx 10^{10}$ at 10^{-2} Hz. There is no known damping mechanism in a high-purity superconductor cooled in a low field that makes this level of Q unachievable. With $Q = 10^{10}$ and the design value $I = 1.5 \times 10^{-4}$ kg m^2, the intrinsic noise of the differential angular accelerometer becomes $S_\alpha^{1/2}(f) = 3.1 \times 10^{-15}$ rad s^{-2} Hz$^{-1/2}$. While this is a demanding sensitivity, the existing SGG has already achieved the required resolution when the sensitivity is expressed in terms of test mass displacement.

Acceleration noise. Figure 8 shows the roll (x), pitch (y), and yaw (z) angular acceleration spectra of ISS derived from the differential GPS data during a reasonably quiet period. The ISS is quietest between 0.003 and 0.03 Hz. The angular acceleration noise at the signal frequency 0.01 Hz is ~ 1×10^{-7} rad s^{-2} Hz$^{-1/2}$. The net CMRR of 10^8 of the detector will reject this noise to 1×10^{-15} rad s^{-2} Hz$^{-1/2}$ per axis.

Figure 9 shows the linear acceleration spectra from MAMS data taken over the same period as the above GPS data. The accelerometer position with respect to the ISS center of mass (c.m.) was (16.472, −0.096, 0.222) m. Along the y- and z-axis, the amplitude of the linear acceleration is within a factor of two from the value, angular acceleration times the lever arm from the c.m. This indicates that the linear acceleration along these axes is mainly the result of the angular acceleration of ISS. This conclusion is confirmed by the fact that the linear acceleration is lowest along the x-axis, which runs within 1 m from the c.m.

With ISS fully assembled, LTMPF is expected to be at about the same distance from the new c.m. of ISS. So we use the spectra shown in Figure 9 to estimate the linear acceleration noise. The detector couples to the y- and z-axis acceleration, 3×10^{-6} m s^{-2} Hz$^{-1/2}$ at 0.01 Hz. With $\varepsilon_L = 5 \times 10^{-11}$ m^{-1}, this noise is reduced to 1.5×10^{-16} m s^{-2} Hz$^{-1/2}$ per axis.

The nonlinearity in the detector coils couples to the y- and z-axis linear acceleration as well as the angular acceleration about the x-axis. Using the nonlinearity coefficient measured in our SGG, we estimate the nonlinearity-induced noise as plotted in Figure 10 before applying feedback to the linear degrees of freedom. While angular acceleration-induced noise is at an acceptable level, 3×10^{-15} m s^{-2} Hz$^{-1/2}$, the linear acceleration-induced noise is five orders of magnitude too high! We solve this problem by actively stiffening the translational modes by five orders of magnitude to a frequency of ~ 100 Hz.

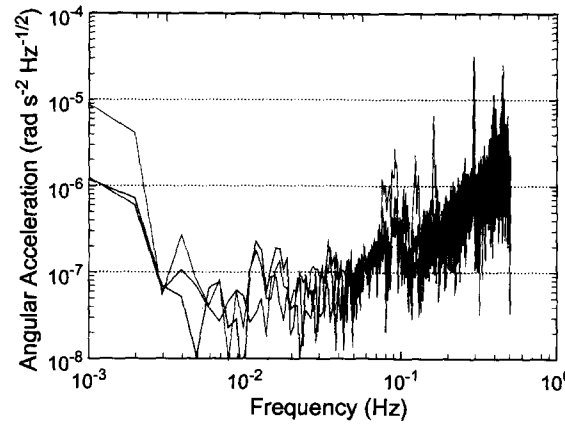

Figure 8. ISS angular acceleration about x- (red), y- (green), z- (blue) axis.

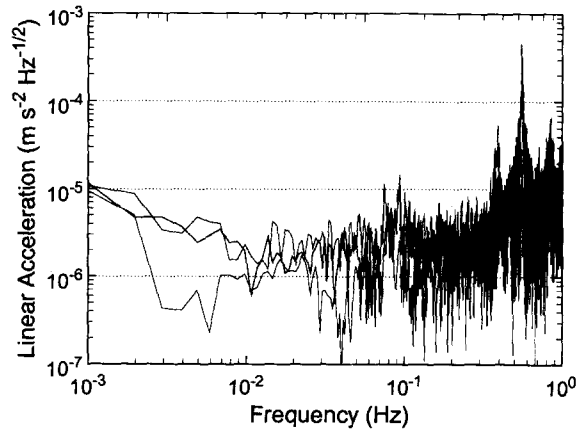

Figure 9. ISS linear acceleration along x- (red), y- (green) and z- (blue) axis.

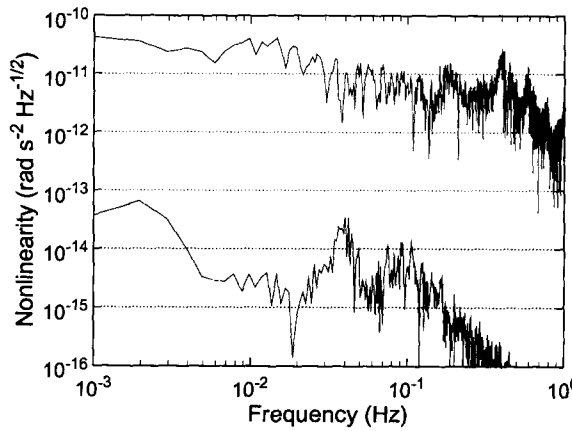

Figure 10. ISS nonlinear coupling to linear (upper) and angular (lower) acceleration.

Gravity noise. Helium tide, which is an important error source for STEP, is absent due to the Earth-fixed orientation of the ISS. Helium sloshing is of minor concern since it is expected to occur at a sufficiently low frequency, ~2.5 mHz. The angular sensing and cylindrical symmetry employed makes the detector very insensitive to gravity noise from helium slosh, the Earth's gravity gradient, and ISS self-gravity, including the activities of astronauts.

The source could couple to the detector gravitationally by magnetostriction and thermal expansion. Fortunately, these effects will occur at the second harmonic and produce mainly a radial distortion of the source, which does not couple to the detector.

Magnetic noise. Cooling and performing the experiment in a low magnetic field will minimize flux creep. LTMPF is equipped with a Cryoperm shield that will help to produce a low-field region. The NdNi will generate a remanent field as it cools through its Curie temperature (~30 K). This field will be trapped by the Magnifer and thus will be kept within the source.

Magnetic crosstalk between the source and the detector is of serious concern. The source is completely wrapped with a Nb shield and all the detector coils are mounted inside a Nb housing. The signal leads to the SQUIDs will be shielded with lead (Pb) tubing. High-purity Nb will be used and heat-treated to bring the material close to a type-I superconductor. The superconducting shield is expected to give over 200-dB isolation (Rigby *et al.*, 1990).

Electric charge effects. The levitated test masses will accumulate electric charge from cosmic rays and from high-energy protons. This charge will induce image charges on the neighboring coils and superconducting ground planes, which produce a net force through asymmetries. This would gradually displace the test masses, possibly deteriorating the CMRR of the detector. SMILE is designed to be inherently insensitive to this effect. By the fundamental nature of electricity, the excess charge always resides on the outer surface of a conductor, and the image charges on the periphery of the test mass cannot exert a torque, again due to its *cylindrical symmetry*! The radial force will couple to angular motion through asymmetry in cylindrical geometry. A cylindricity of 10^{-5} leads to a maximum angular displacement of 5×10^{-9} rad, which is an order-of-magnitude below the level required to maintain a CMRR of 10^5.

The patch-effect potential on the test mass ridges and angular sensing coils could produce a torque. However, most crystal domain boundaries will remain frozen at 2 K and the resulting dc torque will be balanced out upon the CM balance.

Temperature noise. The modulation of the penetration depth of a superconductor with temperature and residual thermal expansion coefficients for different materials give rise to temperature sensitivity in a superconducting accelerometer (Chan and Paik, 1987). These effects lead to a temperature control requirement of $\leq 10^{-4}$ K $Hz^{-1/2}$ for SMILE. A thermal link to the bath will be made to restrict the temperature rise to < 0.1 K above the bath temperature when 1 mW power is produced by the experiment. The temperature of the experiment will be stabilized to ±5 μK.

Total errors. Table 1 combines all the errors. To reduce the random noise to the levels listed, a 90-day integration was assumed. The vibration noise contributes equally to the error budget as the intrinsic noise of the instrument.

Error Source	Error ($\times 10^{-19}$ rad s^{-2})
Random	(90 days)
Intrinsic	11
Vibration	12
Gravity coupling	<1
Magnetic coupling	<5
Electric charge	<1
Others (30% margin)	14
Total	22

Table 1. Error budget.

6. Expected Resolution of SMILE

By equating the total noise with the acceleration signal from spin-mass interaction (Figure 2), we obtain the 1-σ resolution of SMILE plotted in Figure 1. This is compared with the sensitivities of the ground experiment as well as a free-flyer experiment. For the ground experiment, we have computed the sensitivity expected for the prototype source and test masses, which have already been fabricated.

For the free-flyer, we have scaled up the instrument by a factor of two and the noise is averaged over two detectors flown together for 360 days. Another improvement is cooling to 0.05 K by He^3/He^4 dilution refrigerator. Dilution refrigerators with this capability in zero-g are under development at NASA Ames Research Center and elsewhere (Roach and Helvensteijn, 1999). With $f_D = 10^{-3}$ Hz and $Q = 10^{10}$, the intrinsic noise is improved by more than 200. Improvement in the vibration noise will be similar. With a modest improvement of the spin contrast by a factor of two, we obtain an overall improvement of two orders of magnitude over SMILE.

Although the possible detection of the axion at the level allowed by the present theory may take an experiment on a quieter free-flyer, SMILE will search for a generic spin-coupling force in the large parameter space that has never been explored and constitutes an important new test of General Relativity. The ISS experiment will also pave way to an ultimate free-flyer experiment by testing many crucial components of the apparatus.

References

Altarev, I. S. *et al.* (1992), *Phys. Lett. B* **276**, 242.

Bendat, J.S. and Piersol, A. G. (1971), *Random Data: Analysis and Measurement Procedures* (Wiley, New York), Chapter 5.

Blaser, J.-P. *et al.* (1996), *STEP (Satellite Test of the Equivalence Principle)*, Report on the Phase A Study, SCI(96)5.

Chan, H. A. and Paik, H. J. (1987), *Phys. Rev. D* **35**, 3551.

Chan, H. A., Moody, M. V., and Paik, H. J. (1987), *Phys. Rev. D* **35**, 3572.

Graham, D. M. (1987), Ph.D. thesis, University of California, Irvine.

Moody, J. E. and Wilczek, F. (1984), *Phys. Rev. D* **30**, 130.

Moody, M. V., Chan, H. A., and Paik, H. J. (1986), *J. Appl. Phys.* **60**, 4308.

Moody, M. V., Canavan E. R., and Paik, H. J., submitted to *Rev. Sci. Instrum.*

Newman, R. D. (1983), in *Proceedings of the Third Marcel Grossmann Meeting on General Relativity*, ed. H. Ning (North Holland, Amsterdam), p.1497.

Ni, W. T. *et al.* (1999), *Phys. Rev. Lett* **82**, 2439.

Paik, H. J. (1982), in *Proceedings of the Second Marcel Grossmann Meeting on General Relativity*, ed. R. Ruffini (North Holland, Amsterdam), p.1193.

Peccei, R. D. and Quinn, H. (1977), *Phys. Rev. Lett.* **38**, 1440.

Rigby, K. W., Marek, D., and Chui, T. C. P. (1990), *Rev. Sci. Inst.* **2**, 834.

Roach, P. R. and Helvensteijn, B. P. M. (1999), in *Cryocoolers 10*, Ed. R. G. Gross, Jr. (Kluwer/Plenum, New York), p.647.

Shaul, D. *et al.* (1996), *Class. Quantum Grav.* **13**, A107.

Turner, M. S. (1990), *Phys. Rep.* **197**, 67.

Weinberg, S. (1978), *Phys. Rev. Lett.* **40**, 223.

Wilczek, F. (1978), *Phys. Rev. Lett.* **40**, 279.